Dispersion of collective excitations of amorphous and liquid $Zr_{67}Ni_{33}$ alloys

1995 J. Phys.: Condens. Matter 7 1525

(http://iopscience.iop.org/0953-8984/7/8/003)

J. Phys.: Condens. Matter 7 (1995) 1525–1541. Printed in the UK

Dispersion of collective excitations of amorphous and liquid $Zr_{67}Ni_{33}$ alloys

Tomoyasu Aihara Jr and Tsuyoshi Masumoto
Institute for Materials Research, Tohoku University, Katahira 2-1-1, Sendai 980-77, Japan

Received 26 September 1994

Abstract. Molecular dynamics simulations have been performed to study the collective excitation of $Zr_{67}Ni_{33}$ amorphous and liquid alloys with a pair functional potential. The spectrum and the correlation function of the particle current are calculated for longitudinal and transverse modes. The dispersion relation is estimated from the spectrum. It is related to the peak position of the static structure factor and is strongly dependent on temperature at large wavenumbers. The collective excitation is evident for the Zr–Zr correlation but not for the Ni–Ni correlation. The motion of the Zr–Zr correlation is non-localized but that of the Ni–Ni correlation is localized. The sound velocity and the Debye temperature are calculated from the dispersion relation. The calculated power spectrum agrees with the previously reported experimental result. The power spectrum of the Zr atom of the amorphous state is similar to that of the crystal state. On the other hand, the power spectrum of Ni shows an obvious difference between the amorphous and crystal states.

1. Introduction

Atoms in matter are never at rest. The interactions between atoms produce cooperative motion. This atomistic motion is the basis of the macroscopic dynamics of solids and liquids. The phonon, the collective motion with periodicity, is treated as the harmonic oscillator in the periodic structure material in the theory of lattice dynamics. The phonon in a crystal has a zero width and a long lifetime and propagates a long distance. In the macroscopic limitation, it is detected as a sound wave. In the liquid or amorphous structure, there is no long-range periodicity and consequently no reciprocal-lattice point. The direct treatment of lattice dynamics is not applicable to the random structure.

For random-structure materials, neutron inelastic scattering experiments and computer simulations have been performed to clarify the existence of the propagating collective motion having a wavelength of the order of the nearest-neighbour atomic distance. The collective excitation is defined as the peak of the spectrum of the particle current or the dynamic structure factor. The results of these studies show the existence of the phonon dispersion relation for the equilibrium liquid or amorphous state. In these studies, one of the aims is to elucidate the short-wavelength limit of the momentum transfer.

The dynamic structure factor of equilibrium liquid metals and alloys have been measured for Pb [1], Rb [2, 3], Bi [4] and Li–Pb [5] in neutron experiments. The neutron experiment basically gives the dynamical information for the longitudinal mode. The dispersion relation exists up to a somewhat smaller wavenumber than the first peak of the structure factor. The temperature dependence of the dispersion relation has been reported only for liquid Rb metal [2, 3]. The neutron experiments have also been performed for amorphous alloys, e.g. Mg–Zn [6–8], Ca–Mg [9], Zr–Ni [10, 11] and Pd–Si [12]. For amorphous Mg–Zn and

0953-8984/95/081525+17$19.50

Ca–Mg alloys, the dispersion relation was reported to hold throughout a wide wavenumber range. However, the atomistic dynamics of alloys through the glass transition temperature have not been measured yet. Generally, much effort must be made in order to measure the dynamic structure factor for wide wavenumber and frequency ranges. Instead the general vibrational density of states (GVDOS) is usually measured as a function of only frequency.

Theoretical calculations of the collective dynamics in the random-structure material have been performed and some of these were compared with experimental results. For example, Hafner calculated the dynamic structure factor for amorphous $Mg_{70}Zn_{30}$ [13] and $Ca_{70}Mg_{30}$ [9] alloys. He used the recursion method and a realistic model, i.e. pseudopotential-derived interatomic forces. The separation of information on dynamics into the partial parts for each species is difficult experimentally but easy in the simulation. Recently, molecular dynamics (MD) simulations have been performed to study amorphous and liquid materials. MD simulations are based on atomism, and are able to treat the dynamics, the structure and the energy on the atomic level simultaneously. The dispersion relation of liquid metals, e.g. Al [14] and Pb [15], were calculated by MD. For the amorphous state, such MD simulations were performed for alkali halide glasses [16–18].

Metallurgical research on amorphous alloys has been performed to develop its excellent properties from the macroscopic viewpoint [19]. The thermal stability of amorphous alloys is one of their most important properties. In the binary transition metal–metal alloy system, amorphous Zr–Ni alloy is a rare case in which the crystallization temperature is higher than the glass transition temperature under the heating condition. We previously studied MD simulation on amorphous and liquid $Zr_{67}Ni_{33}$ alloys. We clarified the glass transition temperature [20], the temperature dependence of the pair distribution function [20] and the site energy [21]. The experimentally determined glass transition temperature, 652 K [22], is reproduced well by MD simulation as 640 K. The site energy is the locally assigned energy for an individual atom and is based on the concept of the Voronoi polyhedron. The distribution of the site energies shows the partial energy stabilization of the Ni atom in the amorphous state in comparison with the crystal state.

It is of interest to establish the behaviour of the dynamics affected by such an energy peculiarity. Although the dynamics of the amorphous Zr–Ni alloys have been reported by Suck and co-workers [10, 11], details are still unknown. In the present paper, we report a MD simulation for the amorphous and liquid $Zr_{67}Ni_{33}$ alloys. To examine the collective excitations, we calculate the spectrum and correlation function of the particle current for longitudinal and transverse modes at different temperatures. Furthermore, the spectrum of thermal vibrations as single-particle motion is calculated and compared with the result of neutron experiment.

2. Simulation method

The simulated system consists of 640 Zr atoms and 320 Ni atoms with periodic boundary conditions. We use the Nosé constant-temperature method [23] with a modification wherein the volume is varied with object temperature with a constant thermal expansion coefficient of 2.659×10^{-5} K^{-1}. The density of the amorphous state is 7.06 g cm^{-3} at 298 K, in agreement with the experimental value [24]. The calculation is begun by constructing a C16 tetragonal crystal structure ($4 \times 4 \times 5$ lattice cells parallel to the periodic box). The system is first heated well above the melting temperature (T_m = 1393 K) [25], i.e. up to 2000 K, to obtain a homogeneous equilibrium liquid state. The system is quenched quasi-continuously to various object temperatures with a quench rate of 2×10^{14} K^{-1}.

After a subsequent isothermal annealing at the object temperature, statistical analyses were performed. The equations of motion were solved using the fifth-order predictor corrector algorithm of Gear with a time step of 1 fs.

To examine the properties of the metallic bonding system, we use the pair functional potential [26]. Specifically, we employ the potential used by Massobrio *et al* [27]. The total potential energy of the system is written

$$E_{\mathrm{pot}} = \sum_{\alpha=1}^{m}\sum_{i_\alpha}^{N_\alpha}\left[\sum_{\beta=1}^{m}\sum_{j_\beta(\neq i_\alpha)}^{N_\beta} A_{\alpha\beta}\exp\left[-p_{\alpha\beta}\left(\frac{r_{i_\alpha j_\beta}}{d_{\alpha\beta}}-1\right)\right] - \left\{\sum_{\beta=1}^{m}\sum_{j_\beta(\neq i_\alpha)}^{N_\beta}\xi_{\alpha\beta}^2\exp\left[-2q_{\alpha\beta}\left(\frac{r_{i_\alpha j_\beta}}{d_{\alpha\beta}}-1\right)\right]\right\}^{1/2}\right] \tag{1}$$

where $r_{i_\alpha j_\beta}$ is the distance between i_α and j_β atoms. The latter functional term represents the many-body interactions in metallic bonding matter. They fitted the potential to reproduce the thermodynamic and elastic properties of the crystal structures [27]. The pair functional potential allows for quantitative simulation of the ductile properties of a metallic crystal [28].

The dynamics of the atoms in materials are classified into two categories, i.e. mutually collective motion and single-atom motion. The particle current describes the time-dependent spatial collective correlation. The spatial Fourier component of the time-dependent particle current for species α is

$$j_\alpha(Q,t) = \sum_{i_\alpha=1}^{N_\alpha} v_{i_\alpha}(t)\exp[-iQ\cdot r_{i_\alpha}(t)] \tag{2}$$

where t is the time, $r_{i_\alpha}(t)$ the time-dependent coordinate of the atom i_α, $v_{i_\alpha}(t)$ the velocity, Q the wavenumber vector and N_α the number of species α. This particle current is also described by the angular frequency ω by the Fourier transform with time:

$$j_\alpha(Q,\omega) = \lim_{T\to\infty}\frac{1}{\pi}\int_0^T j_\alpha(Q,t)\exp(i\omega t)\,\mathrm{d}t. \tag{3}$$

This particle current in the reciprocal lattice consists of two modes. In the longitudinal mode, the velocity vector is parallel to the wavenumber vector. In the transverse mode, they are perpendicular. The Ashcroft–Langreth-type spectrum of the particle current for α–β atom correlation is calculated using equation (3). The spectrum of the longitudinal mode is defined as [29–31]

$$C_{\mathrm{l}}(Q,\omega) = \frac{\pi}{T\sqrt{N_\alpha N_\beta}}|\{k\cdot j_\alpha(Q,\omega)\}\{k\cdot j_\beta(Q,\omega)\}^* + \{k\cdot j_\alpha(Q,\omega)\}^*\{k\cdot j_\beta(Q,\omega)\}| \tag{4}$$

and the transverse mode is defined as

$$C_{\mathrm{t}}(Q,\omega) = \frac{\pi}{T\sqrt{N_\alpha N_\beta}}|\,\mathrm{Tr}\langle[k\times j_\alpha(Q,\omega)]\cdot[k\times j_\beta(Q,\omega)]^* + [k\times j_\alpha(Q,\omega)]^*\cdot[k\times j_\beta(Q,\omega)]\rangle| \tag{5}$$

where $k = Q/|Q|$. The Bhatia–Thornton-type number–number density spectrum is calculated from

$$C_{NN}(Q,\omega) = x_A C_{AA}(Q,\omega) + x_B C_{BB}(Q,\omega) + 2\sqrt{x_A x_B} C_{AB}(Q,\omega) \tag{6}$$

where x_A is the concentration of the A atoms. The correlation function of the particle current is calculated using

$$C(Q,t) \equiv \langle j(Q,t) \cdot j(Q,0) \rangle = \int_0^{\omega_{max}} C(Q,\omega)\cos(\omega t)\,d\omega. \tag{7}$$

This inverse Fourier transform equation saves computation time in comparison with the direct calculation of the correlation function.

In the isotropic random structure, all the wavevector-dependent functions are affected not in the direction but in the magnitude of the wavevector. We calculated the dynamic structure factor for three orthogonal wavevectors and averaged them. The wavevectors are restricted as

$$Q = \frac{2\pi}{L} n \tag{8}$$

where n is the orthogonal integer vector and L the length of the MD cell.

The power spectrum of the velocity autocorrelation function is defined as

$$Z_\alpha(\omega) = \frac{2}{\pi} \int_0^\infty \sum_{i_\alpha=1}^{N_\alpha} \langle v_{i_\alpha}(0) \cdot v_{i_\alpha}(t) \rangle \cos(\omega t)\,dt. \tag{9}$$

It corresponds to the GVDOS measured in the neutron inelastic scattering experiment with incoherent approximation. The GVDOS of the $Zr_{67}Ni_{33}$ alloy is calculated as

$$G_{DOS}(\omega) = 0.325 Z_{Zr}(\omega) + 0.675 Z_{Ni}(\omega) \tag{10}$$

where the weighting is calculated from the scattering length, the composition, the mass of the atom and the Debye–Waller factor [32].

3. Results and discussion

3.1. Structure factor

Before treating the dynamical properties, we examine the static structure of the system in the amorphous state. Although there is no reciprocal lattice or Brillouin zone in the random-structure materials, short-range or medium-range order exists in the random structure. The structure factor is calculated as the spatial Fourier transform of the pair distribution function. The simulated x-ray weighted structure factor of amorphous $Zr_{67}Ni_{33}$ alloy at 298 K is shown in figure 1 with the experimental results for amorphous $Zr_{65}Ni_{35}$ alloy from the work of Lee *et al* [33]. The structure factor takes the first maximum at the wavenumber $Q_0 = 26\ nm^{-1}$. The basic configuration of the static structure does not change with temperature [20].

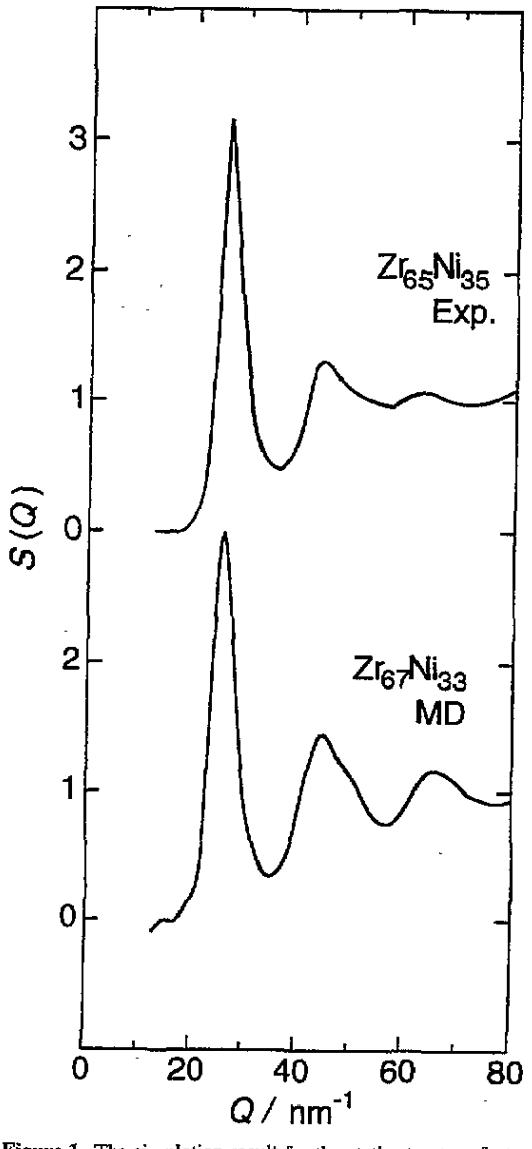

Figure 1. The simulation result for the static structure factor at 298 K compared with the result obtained by x-ray measurements [33].

3.2. Spectrum of particle current

The calculations of the particle current are performed at four different temperatures, i.e. 100 K (low-temperature amorphous state), 500 K (high-temperature amorphous state), 700 K (supercooled liquid state just above the glass transition temperature $T_g = 640$ K [20]) and 1400 K (equilibrium liquid state). The longitudinal mode spectrum of the particle current is related to the dynamic structure factor $S(Q, \omega)$, which is measured in the neutron inelastic scattering experiment. The relation is

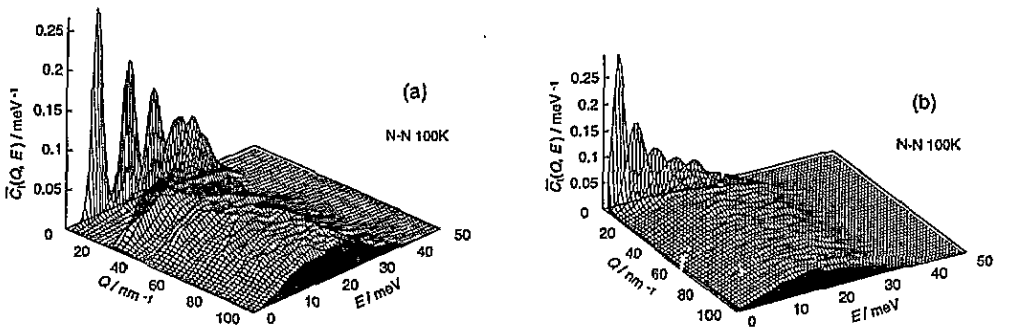

Figure 2. The Bhatia–Thornton-type normalized spectrum of the particle current for the number–number density correlation at 100 K for the amorphous state in a 3D representation: (a) longitudinal mode, $\bar{C}_l(Q, E)$; (b) transverse mode $\bar{C}_t(Q, E)$.

$$C_l(Q, \omega) = \frac{\omega^2}{|Q|^2} S(Q, \omega). \tag{11}$$

Figure 2(a) shows the Bhatia–Thornton-type spectra of the particle current for the number–number density correlation at 100 K in the amorphous state, as a three-dimensional plot. The angular frequency ω is indicated as the energy ($E = \hbar\omega$), where $\hbar$ is the Planck constant. We normalized all spectra by the energy at each wavenumber. The longitudinal mode spectrum $\bar{C}_l(Q, E)$ in figure 2(a), shows the Brillouin-zone-like configuration up to the wavenumber $2Q_0$ and a broadened shape at large wavenumbers. The peak for collective excitation is sharp at long wavelengths. The peak energy increases with increasing wavenumber up to $Q_0/2$. The peak position shifts to the low-energy side near a peak in the static structure factor, which corresponds to a broadened reciprocal-lattice point. The spectrum for the longitudinal mode is zero above 40 meV and at 0 meV. The transverse mode spectrum $\bar{C}_t(Q, E)$ in figure 2(b) show well defined peaks for collective excitation only for small wavenumbers, and a broadened shape above 20 nm^{-1}. The correlation of the spectrum for the transverse mode is zero above 40 meV; however, it is a finite value near 0 meV at large wavenumbers.

The Ashcroft–Langreth-type partial spectra at 100 K are shown in figure 3. The peak height for the Ni–Ni correlation is smaller than the half-height for the Zr–Zr correlation for the longitudinal and transverse modes. The dispersion relation is evident for the Zr–Zr correlation but not for the Ni–Ni correlation. The sharp peak of the spectrum indicates the existence of the periodic collective motion. If the atoms move independently, i.e. the motion is localized, there is a broadened peak in the spectrum. Then it is concluded that the motion of the Zr–Zr correlation is non-localized but that of the Ni–Ni correlation is localized.

The spectra for the number–number correlation of the equilibrium liquid state (1400 K) are shown in figure 4. The collective excitation peak is slightly broadened for both modes. These behaviours show that the lifetime of the phonon becomes short with increasing temperature. For the longitudinal mode, the peak positions shift to the high-energy side at large wavenumbers, and the zero-energy correlation becomes strong near the wavenumber Q_0. For the transverse mode, the peak positions shift to the low-energy side at large wavenumbers. We also performed calculations for 500 and 700 K. These spectra show the intermediate configuration between 100 and 1400 K.

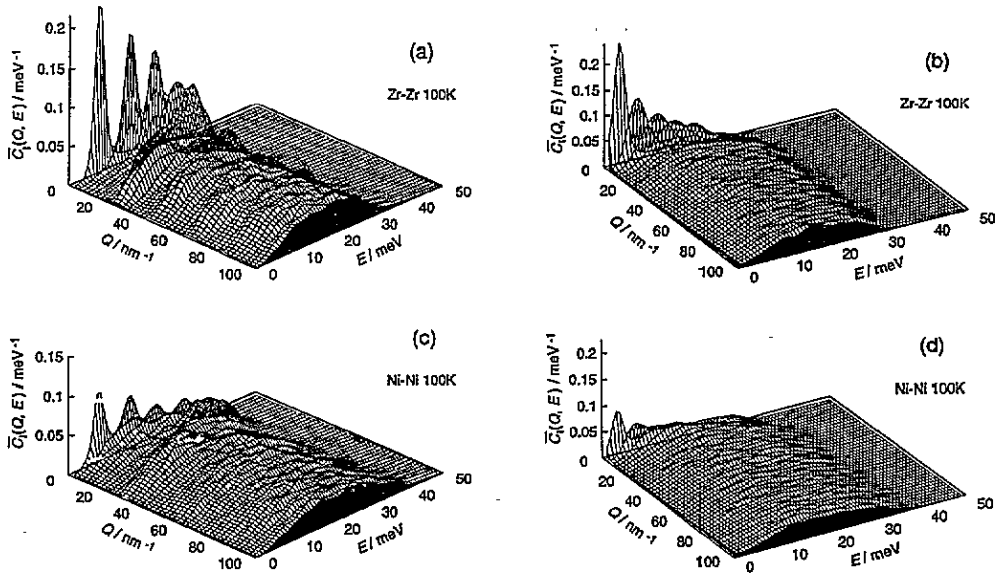

Figure 3. The Ashcroft–Langreth-type normalized partial spectrum of the particle current at 100 K: (a) longitudinal mode for Zr–Zr correlation; (b) transverse mode for Zr–Zr correlation; (c) longitudinal mode for Ni–Ni correlation; (d) transverse mode for Ni–Ni correlation.

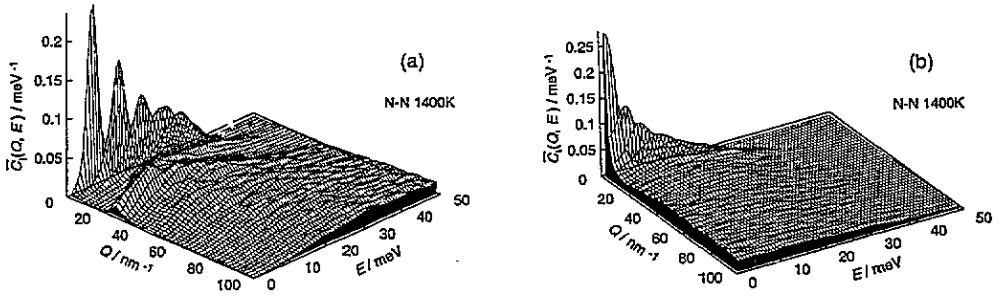

Figure 4. The Bhatia–Thornton-type normalized spectrum of the particle current for the number–number density correlation at 1400 K for the equilibrium liquid state: (a) longitudinal mode $\bar{C}_l(Q, E)$; (b) transverse mode $\bar{C}_t(Q, E)$.

3.3. Dispersion law

We define the dispersion relation as the peak position in the spectrum of the particle current for number–number correlation, similarly to the result of the neutron experiment for liquid Rb [2,3]. The simulated dispersion relation is plotted in figure 5(a) for the longitudinal mode and in figure 5(b) for the transverse mode.

For the longitudinal mode, periodicity is observed below $2Q_0$. The peak value of the energy at the first maximum ($Q = Q_0/2$) is higher than that at the second maximum ($Q = 3Q_0/2$). The energy range of the present result is comparable with that of the amorphous $Ca_{70}Mg_{30}$ [9] and $Mg_{70}Zn_{30}$ [13] alloys. Below $3Q_0/2$, the peak values of the energy decrease slightly with increasing temperature. The peak energy for 100 K saturates to 15 meV at large wavenumbers. It obviously increases with increasing temperature. Suck

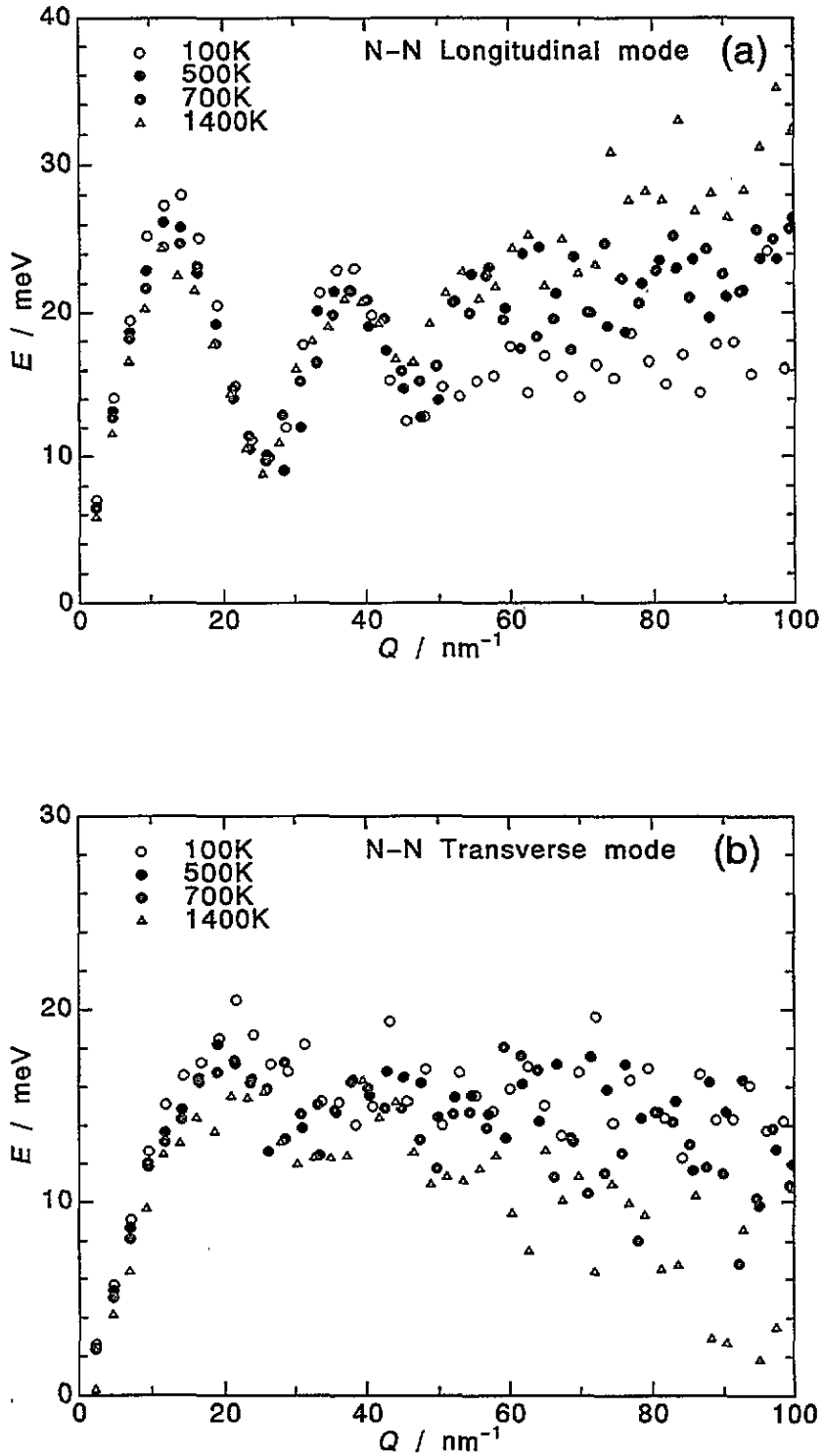

Figure 5. Dispersion law of propagating collective excitations for the number–number density correlation as a function of temperature: (a) longitudinal mode; (b) transverse mode.

et al [10] reported the dispersion relation for amorphous $Zr_{76}Ni_{24}$ alloy from 22 to 28 nm^{-1} as the maximum and shoulders in the total dynamic structure factor using neutron inelastic scattering. Their results show that the minimum energy at Q_0 is 1.8 meV, which is low in comparison with other alloys. On the other hand, the minimum energy at Q_0 is about 10 meV in the present simulation. The study of the amorphous $Ca_{70}Mg_{30}$ alloy by Hafner [9] shows that the minimum value at Q_0 from the neutron experiment is lower than the simulated value. The MD result consists of pure longitudinal one-phonon scattering. Hafner [9] explains that this energy difference arises from other collective low-energy modes.

For the transverse mode, the energy increases with increasing wavenumber and reaches a maximum at $Q = 20$ nm^{-1}. The maximum value of the energy for the transverse mode is about two thirds of that for the longitudinal mode and decreases slightly with increasing temperature. At large wavenumbers, the peak energy saturates to 15 meV at 100 K. It obviously decreases with increasing temperature.

The dispersion relation is fitted by the sinusoidal function at small wavenumbers. The longitudinal velocity v_l of sound and transverse velocity v_t of sound are calculated from the slope at the zero-energy limit. Figure 6 shows the estimated sound velocities at each temperature. The longitudinal sound velocity decreases with increasing temperature. The sound velocity has not yet been reported for the Zr–Ni random structure. However, the sound velocities of pure Zr and Ni crystalline metals at room temperature have been reported. The longitudinal sound velocity of Zr is 4359 m s^{-1}, and that of Ni is 5806 m s^{-1}; the transverse sound velocity of Zr is 1945 m s^{-1} and that of Ni is 3076 m s^{-1} [34]. The sound velocities estimated from the MD simulation for the transverse mode are lower than those for the composition average of the pure element crystal by 16%. On the other hand, the MD result for the longitudinal mode is lower than the averaged value by 1%.

The phonon is related to the thermal properties. A study concerning this point has been reported by Choy *et al* [35] for amorphous Zr–Cu, Ti–Cu and Fe-based alloys. They defined the average sound velocity as

$$v_m = \left[\frac{1}{3}\left(\frac{2}{v_t^3} + \frac{1}{v_l^3}\right)\right]^{-1/3}. \tag{12}$$

The low-temperature specific-heat data give the Debye temperature Θ, from which the sound velocity v_Θ is calculated as

$$v_\Theta = \frac{k}{\hbar}\left(\frac{\bar{m}}{6\pi^2\rho}\right)^{1/3}\Theta \tag{13}$$

where k is the Boltzmann constant, $\bar{m}$ is the average mass of an atom and ρ is the density. They found that v_Θ is lower than v_m by 4–18% for metal–metal amorphous alloys. Gronert *et al* [36] estimated the Debye temperature of amorphous $Zr_{67}Ni_{33}$ alloys as 217 K from the measurement of the low-temperature specific heat. In the present simulation, the Debye temperature calculated from the averaged sound velocity is 254 ± 11 K, which is higher than the value obtained by Gronert *et al* by 17% and satisfies the empirical relation of Choy *et al*.

3.4. Correlation function of particle current

The normalized correlation functions of particle current for the longitudinal mode at 100 K are shown in figure 7(a) and at 1400 K in figure 7(b). The plots of correlation functions are performed every 20 fs. Below the wavenumber $Q_0/2 = 13$ nm^{-1}, the longitudinal

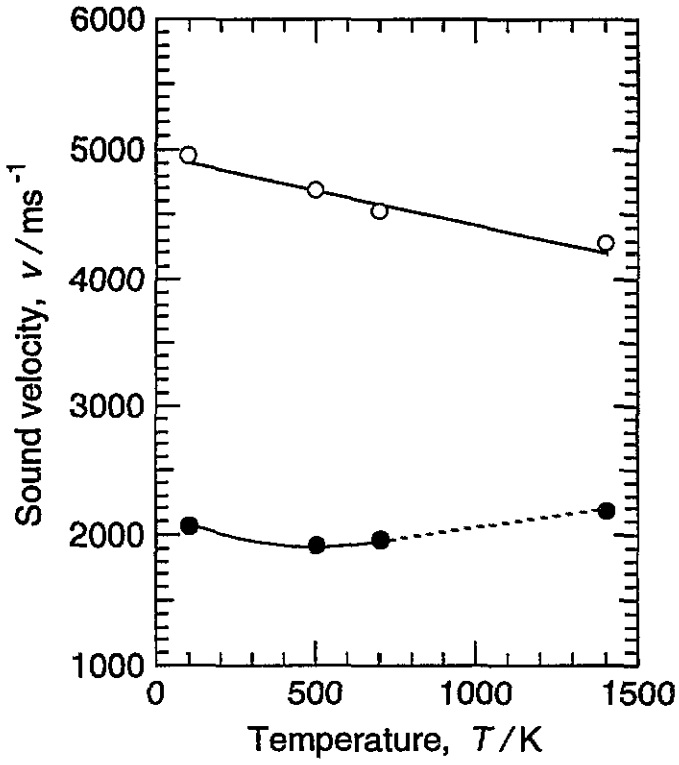

Figure 6. Temperature dependence of the sound velocity for the longitudinal (○) and transverse (●) mode.

correlation functions $\tilde{C}_l(Q,t)$ oscillate harmonically, reflecting the dispersion relation, and slowly attenuate in both amorphous and liquid states. Over $Q_0/2$, the anharmonicity becomes strong and attenuation becomes fast, especially near the peak in the static structure factor. Although the depth of back scattering at Q_0 decreases with increasing temperature, the basic configuration for the longitudinal correlation function is not strongly dependent on temperature. The longitudinal mode correlation functions at 500 and 700 K show the intermediate configuration between 100 and 1400 K.

The normalized correlation functions of particle current for the transverse mode at 100 K are shown in figure 8(a) and at 1400 K in figure 8(b). For the amorphous state, the transverse correlation functions $\tilde{C}_t(Q,t)$ oscillate harmonically, reflecting the dispersion relation at the lowest wavenumber. The correlation function becomes anharmonic and shows fast attenuation with increasing wavenumber. Unlike the longitudinal mode, a strong wavenumber dependence over $Q_0/2$ does not appear for the configuration of the transverse correlation function. Although the depth of back scattering over $Q_0/2$ becomes shallow with increasing temperature, the transverse-mode correlation functions at 500 and 700 K are similar to that at 100 K. For the equilibrium liquid state, the correlation function shows anharmonic behaviour even at the lowest wavenumbers. This means that the transverse collective motion in the equilibrium liquid state is anharmonic in comparison with that in the amorphous state.

The difference in the partial parts for the collective excitation is evident from the correlation function. Figure 9 shows the Ashcroft–Langreth-type partial correlation function

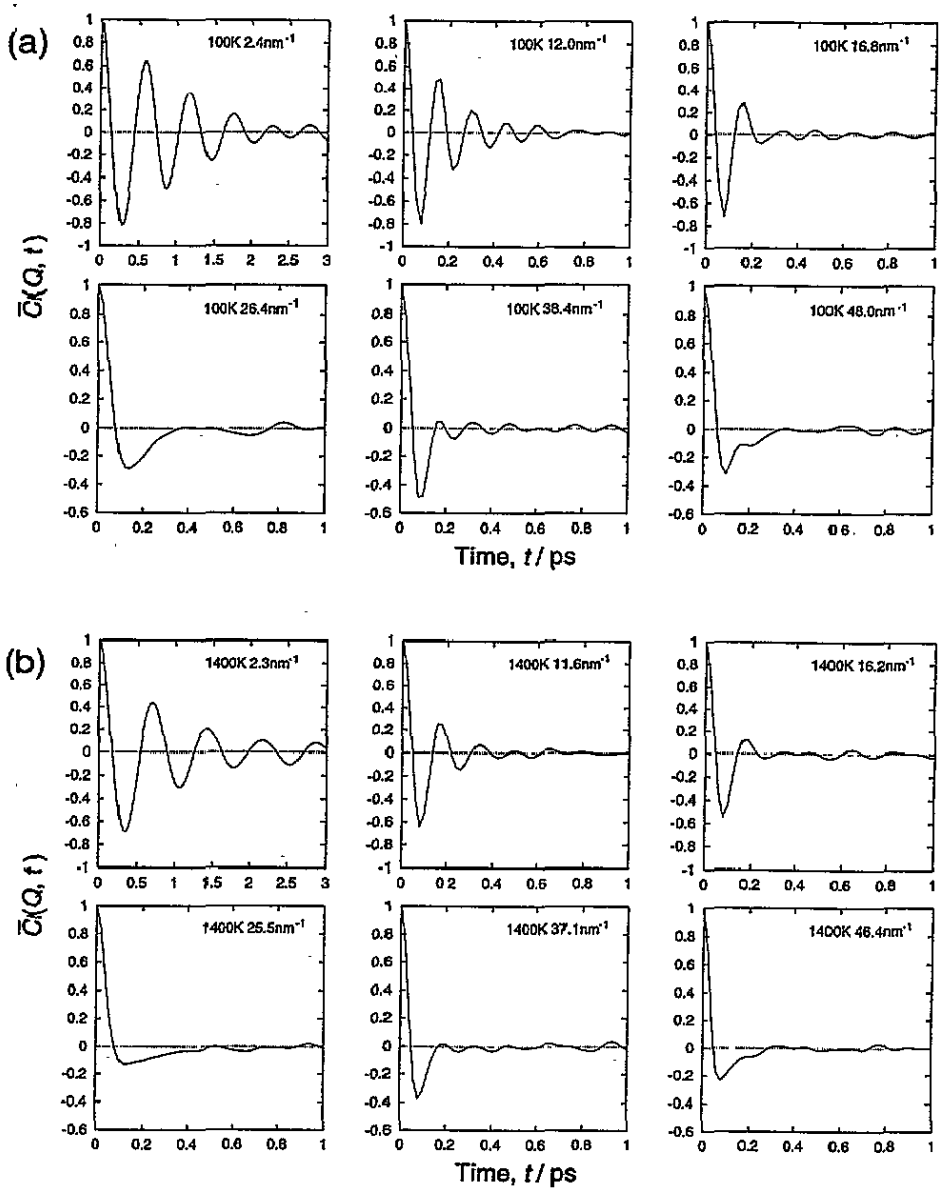

Figure 7. The normalized correlation function of the longitudinal mode particle current for the number–number density correlation $\bar{C}_l(Q, t)$: (a) 100 K; (b) 1400 K.

of the particle current at 100 K and 2.4 nm^{-1} for the longitudinal and transverse modes. The configuration of the Zr–Zr correlation functions for both modes are similar to that of the number–number correlations. For the transverse mode, however, a slight notch is observed near 0.1 ps. The Zr–Zr correlation for the longitudinal and transverse modes basically consists of low-frequency corrective excitation. On the other hand, the Ni–Ni correlation functions at long wavelegnths show low- and high-frequency collective excitations. The low-frequency motion is the same frequency as the Zr–Zr correlation. However, the attenuation of this motion is fast. The high-frequency motion at small wavenumbers, the

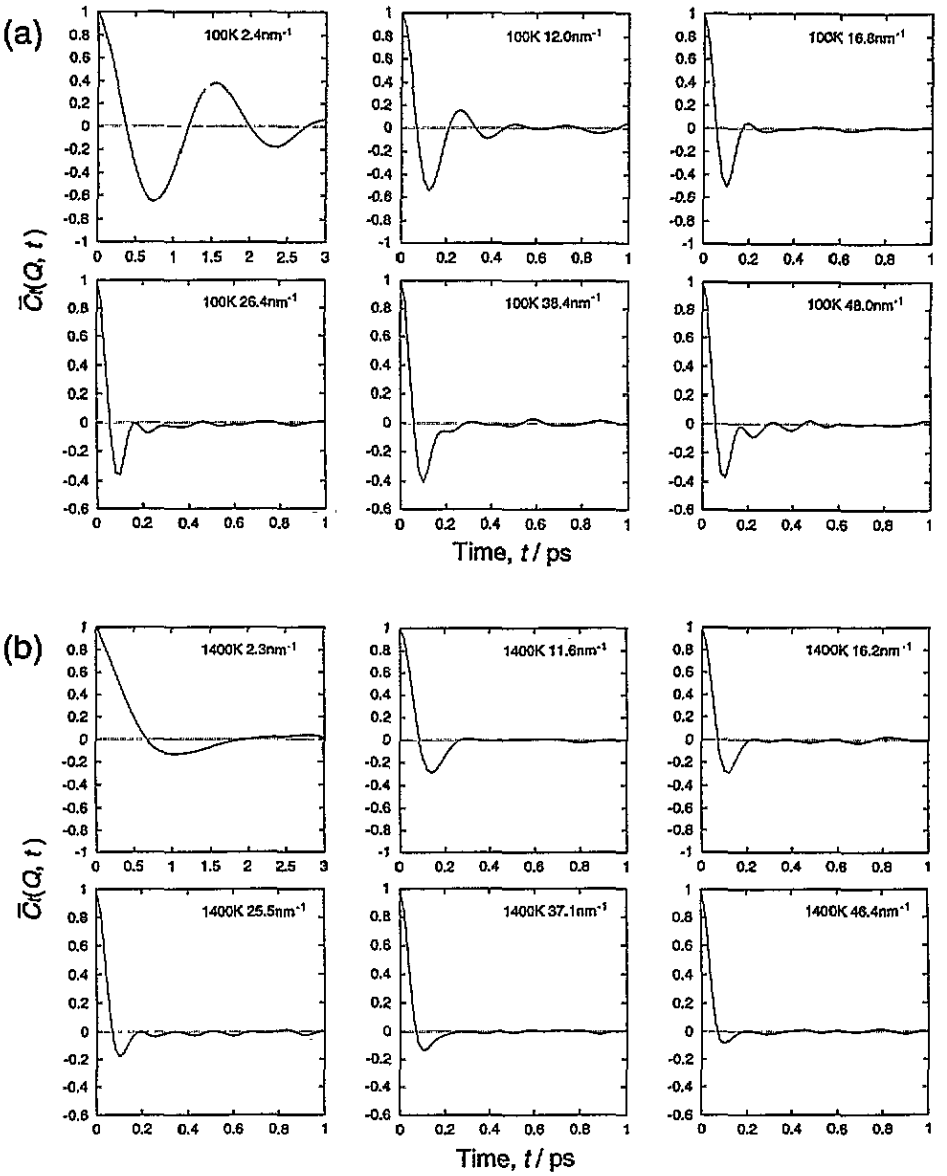

Figure 8. The normalized correlation function of the transverse mode particle current for the number–number density correlation $\bar{C}_t(Q, t)$: (a) 100 K; (b) 1400 K.

frequency of which is the same as at large wavenumbers, is evident for both modes in the Ni–Ni correlation. Although we present only 100 K results, such high-frequency oscillations are observed up to 1400 K. This anomalous behaviour for the Ni–Ni correlation means that the Ni–Ni motion is localized.

3.5. Single-particle motion

We analyse the periodic single-particle motion. The GVDOS of the amorphous state at 298 K is shown in figure 10. The simulated result is compared with the neutron inelastic

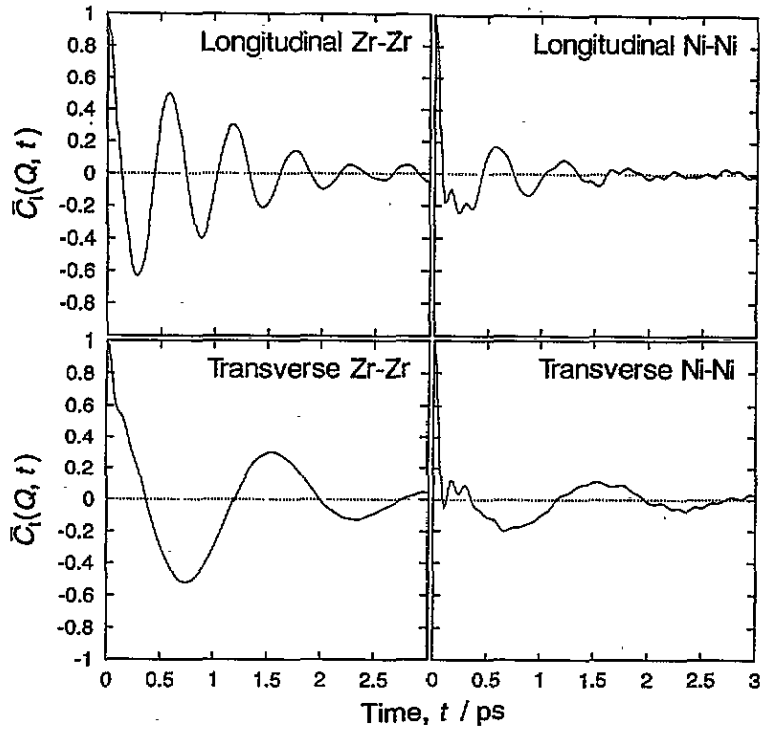

Figure 9. The normalized correlation function of the particle current for the Zr–Zr and Ni–Ni correlation for the longitudinal mode $\bar{C}_l(Q,t)$ and the transverse mode $\bar{C}_t(Q,t)$ at 2.4 nm^{-1} and 100 K for the amorphous state.

scattering data at room temperature obtained by Suck [11]. Each curve represents the difference between the GVDOSs of amorphous and crystal alloys, defined by

$$\Delta G_{\mathrm{DOS}}(\omega) = G_{\mathrm{DOS}}^{\mathrm{amorphous}}(\omega) - G_{\mathrm{DOS}}^{\mathrm{crystal}}(\omega). \tag{14}$$

The background in the neutron experiment is neglected in this operation. The MD result basically agrees with the experimental result, especially in the high-frequency region. The separated GVDOSs, i.e. power spectra obtained by MD, are shown in figure 11. The profiles of the power spectrum for Zr are similar for the amorphous and the crystal state. On the other hand, a large difference is observed for those of the Ni atom. The power spectrum of Ni in the crystal state has a sharp peak at 27 meV. The Ni spectrum in the amorphous state has no sharp peak. The high-frequency vibration of the Ni atom over 30 meV is evident in the amorphous state but is not observed in the crystal state. The difference between the GVDOSs of the crystal and amorphous states is mainly caused by the Ni atom behaviour.

The GVDOSs have been reported from experiments on other amorphous alloys. In the $Mg_{70}Zn_{30}$ alloy, the GVDOS of the amorphous state is similar to that of the crystal state [7]. The GVDOS of $Pd_{79}Si_{21}$ amorphous alloy has two broad peaks [12]. Peak splitting is caused by the low vibrational frequency of metal atom motion and the high frequency of metalloid atom motion. Although the Zr–Ni alloy is a metal–metal system, the Ni species behave differently. The high-frequency vibration is evidence of the existence of the atom in the steep potential well. We have reported the structural and energy difference between

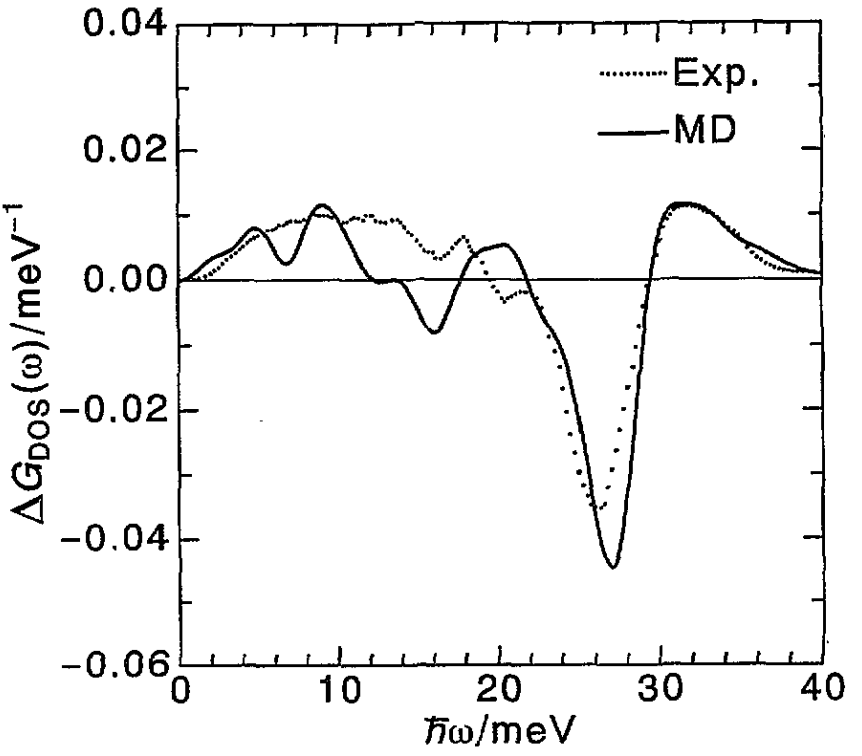

Figure 10. Differences in the GVDOS of the amorphous $Zr_{67}Ni_{33}$ alloy and the C16 Zr_2Ni intermetallic compound at room temperature. The experimental data were reported by Suck [11] using neutron inelastic scattering.

the Zr–Ni amorphous and crystal states [21]. The Ni–Ni distance in the amorphous phase is shorter than in the crystal phase. The Ni–Ni coordination number in the amorphous phase is 3.0 and that in the crystal phase is 2. The distribution of the site energies of Zr atoms in the amorphous phase is usually higher than in the crystal phase. On the other hand, the distribution of the site energies of Ni atoms in the amorphous phase is partially lower than in the crystal phase. The structural and energy differences affect the vibrational dynamics, especially for Ni species.

4. Conclusions

We have performed a MD simulation for the amorphous and liquid $Zr_{67}Ni_{33}$ alloys with a pair functional potential. The present results have been compared with those of the previously reported scattering experiments.

The first peak of the structure factor of the random phase is located at $Q_0 = 26\ nm^{-1}$. The spectrum, which gives the dispersion relation, and the correlation function of the particle current were calculated for longitudinal and transverse modes. For the longitudinal mode, clear collective excitation is observed for wavenumbers $Q < 2Q_0$. The dispersion relation shows minima, and the correlation function indicates the anharmonic configuration, at the peak position of the static structure factor. For the transverse mode, the dispersion relation

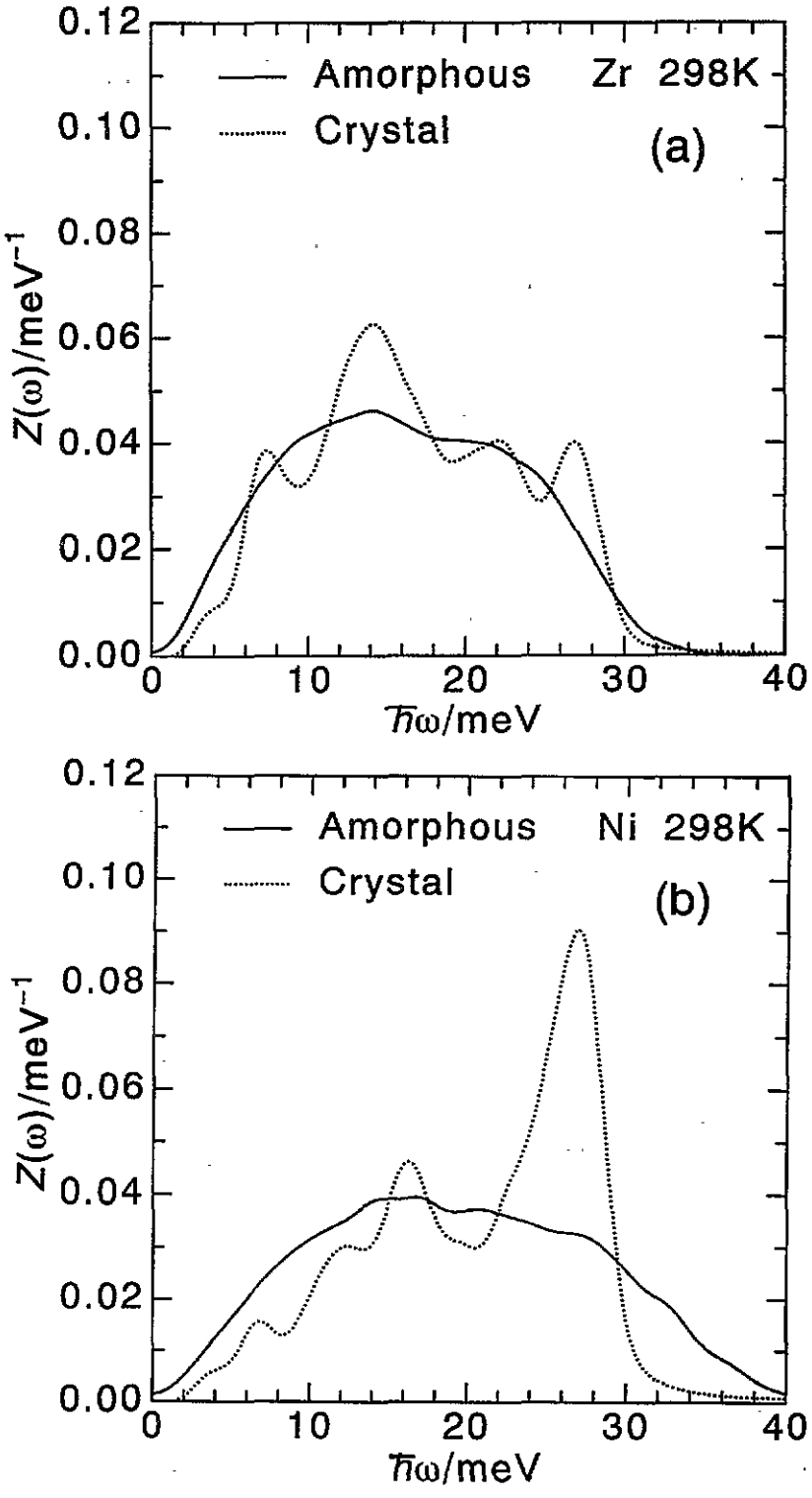

Figure 11. Power spectrum of the velocity autocorrelation function for the amorphous $Zr_{67}Ni_{33}$ alloy and the C16 Zr_2Ni intermetallic compound at 298 K: (a) Zr atom; (b) Ni atom.

is evident only at small wavenumbers below $Q = 20$ nm^{-1}. However, the transverse correlation function at the smallest wavenumber becomes anharmonic for the equilibrium liquid state. The energy of the dispersion relation at large wavenumbers increases for the longitudinal mode and decreases for the transverse mode with increasing temperature. The sound velocity obtained from the dispersion relation gives the Debye temperature which satisfies the experimental value. Collective excitation is evident for the Zr–Zr correlation but not for the Ni–Ni correlation. The motion of the Zr–Zr correlation is non-localized but that of the Ni–Ni correlation is localized.

The spectrum of single-particle vibrational motion is calculated as a GVDOS for the amorphous and crystal states. This simulated result agrees with the previously reported neutron inelastic scattering result. The power spectrum, i.e. the partial GVDOS, of the Zr atom of the amorphous state is similar to that of the crystal state. The power spectrum of the Ni atom of the amorphous state shows a higher-frequency vibration than that of the crystal state. This high-frequency vibration means that the Ni atom is located in a steep potential well.

Acknowledgments

The authors would like to thank Professors Y Kawazoe and K Suzuki for helpful discussion. The numerical calculations were performed on the NEC SX-3R at the Computer Center, Tohoku University and supercomputing system HITAC S3800/380 at the Institute for Materials Research (IMR), Tohoku University. The authors are indebted to the Information Science Group of IMR, Tohoku University, for partial support. The authors acknowledge gratefully partial support of this work by Grants-in-Aid for Scientific Research on the Priority Area of Development of Micro-Heat Transfer for Manufacturing and Processing of New Materials (grant 06230201) and Computational Physics as New Frontier in Condensed Matter Research (grant 05215208).

References

[1] Soderstrom O 1981 *Phys. Rev.* A **2** 785
[2] Winter R, Pilgrim C and Hensel F 1991 *J. Physique IV* **1** C5 45
[3] Copley J R D and Rowe J M 1974 *J. Phys. Soc. Japan* **32** 49
[4] Shibata K, Hishibo S and Fujisita H 1984 *J. Phys. Soc. Japan* **53** 899
[5] Soltwisch M, Quitmann D, Ruppersberg H and Suck J B 1983 *Phys. Rev.* B **28** 5583
[6] Suck J B, Rudin H, Guntherodt H J and Beck H 1980 *J. Phys. C: Solid State Phys.* **13** L1045
[7] Suck J B, Rudin H, Guntherodt H J and Beck H 1981 *J. Phys. C: Solid State Phys.* **14** 2305
[8] Suck J B, Eagelstaff P A, Robinson R A, Sivia D S and Taylor A D 1992 *J. Non-Cryst. Solids* **150** 245
[9] Hafner J 1983 *Phys. Rev.* B **27** 678
[10] Suck J B, Rudin H and Guntherodt H J 1985 *Proc. 5th Int. Conf. on Rapidly Quenched Metals* ed S Steeb and H Warlimont (Amsterdam: North-Holland) p 471
[11] Suck J B 1989 *Dynamics of Disordered Materials* ed D Richter, A J Dianoux, W Petry and J Teixeria (Berlin: Springer) p 182
[12] Shibata K, Mizuseki H, Finney J L and Suzuki K 1992 *J. Non-Cryst. Solids* **150** 251
[13] Hafner J 1983 *J. Phys. C: Solid State Phys.* **16** 5773
[14] Ebbsjo I, Kinelland T and Waller I 1980 *J. Phys. F: Met. Phys.* **13** 1865
[15] Larsson K E, Dzugutov M and Gudowski W 1990 *Il Nuovo Cimento* D **12** 559
[16] Kinugawa K 1992 *J. Chem. Phys.* **97** 8581
[17] Kinugawa K, Kadono K and Tanaka H 1992 *J. Non-Cryst. Solids* **150** 281
[18] Okazaki S, Miyamoto Y and Okada I 1992 *Phys. Rev.* B **45** 2055
[19] Masumoto T 1994 *Mater. Sci. Eng.* A **179–80** 8

[20] Aihara T Jr, Aoki K and Masumoto T 1993 *Scr. Metall.* **28** 511
[21] Aihara T Jr, Aoki K and Masumoto T 1994 *Mater. Sci. Eng.* A **179–180** 256
[22] Altounian Z, Guo-hua T and Strom-Olsen J O 1983 *J. Appl. Phys.* **54** 3111
[23] Nosé S 1984 *J. Chem. Phys.* **81** 511
[24] Altounian Z and Strom-Olsen J O 1983 *Phys. Rev.* B **27** 4149
[25] Massalsky T B (ed) 1991 *Binary Alloy Phase Diagrams* 2nd edn (Metals Park, OH: American Society for Metals)
[26] Carlsson A E 1990 *Solid State Physics* vol 43 (New York: Academic) p 1
[27] Massobrio C, Pontikis V and Martin G 1991 *Phys. Rev.* B **41** 10486
[28] Daw M S, Foils S M and Baskes M I 1993 *Mater. Sci. Rep.* **9** 251
[29] Hansen J P and McDonald I R 1986 *Theory of Simple Liquids* 2nd edn (London: Academic)
[30] Kaneko Y and Ueda A 1989 *Phys. Rev.* B **39** 10281
[31] Roux J N, Barrat J L and Hansen J P 1989 *J. Phys.: Condens. Matter* **1** 7171
[32] Suzuki K 1987 *Methods of Experimental Physics, Part B, Neutron Scattering* ed K Skold and D L Price (London: Academic) p 243
[33] Lee A, Etherington G and Wagner C N J 1984 *J. Non-Cryst. Solids* **61–62** 349
[34] Schramm K H 1962 *Z. Metallk.* **53** 729
[35] Choy C L, Tong K W, Wong H K and Leung W P 1991 *J. Appl. Phys.* **70** 4919
[36] Gronert H W, Herlach D M, Schroder A, Berg R and Lohneysen H 1986 *Z. Phys.* B **63** 173